AIAA JOURNAL
Vol. 38, No. 1, January 2000

Turbulence Effect on Frequency Characteristics of Unsteady Motions in Wake of Wing

Rong F. Huang* and Han W. Lee†
National Taiwan University of Science and Technology, Taipei 106, Taiwan, Republic of China

The influences of the freestream turbulence intensity on the frequency characteristics of the instability wave and vortex shedding in the wake of a NACA 0012 wing model are studied experimentally. The functional relationships among the Strouhal, Roshko, and Reynolds numbers in the viscous-effect-dominated and the inertial-effect-dominated regimes are obtained. The freestream turbulence has apparent effect on the Strouhal and Roshko numbers in the regimes of instability wave and laminar and subcritical vortex-shedding modes that are obtained at low Reynolds numbers. However, at large Reynolds numbers in the supercritical vortex-shedding mode, particularly at large angles of attack, the effect of freestream turbulence intensity on the frequency selection is not significant. For the instability wave, the Roshko number decreases with the increase of freestream turbulence and then approaches constant values when the freestream turbulence intensity is larger than a critical value between 0.45 and 0.5%. However, the Strouhal number of the vortex shedding of laminar and subcritical modes increases significantly with an increase of turbulence intensity and then decreases when the freestream turbulence intensity is larger than a critical value between 0.45 and 0.5%. The change of the characteristic surface flow modes may contribute to the dominant mechanism of the existence of critical freestream turbulence intensity.

Nomenclature

C = chord length of wing, 6 cm
d = length of wing-section projection on cross-stream plane
f = frequency of instabilities in wake region, Hz
$\mathcal{L}$ = distance in X direction measured from mesh screen
M = mesh size of turbulence generation screen
Re_c = Reynolds number based on chord length of wing, $u_w C/\nu$
Re_d = Reynolds number based on cross-stream projection of wing section, $u_w d/\nu$
Ro_d = Roshko number of vortex shedding, fd^2/ν
Sr_d = Strouhal number of vortex shedding, fd/u_w
T = freestream turbulence intensity
u = x component of local instantaneous velocity
u_w = average freestream velocity
X = streamwise coordinate, originated from leading edge of wing model on root-plane
Y = spanwise coordinate, originated from leading edge of wing model on root-plane
Z = crossflow coordinate, originated from leading edge of wing model on root-plane
α = root angle of attack
ν = kinetic viscosity of air stream
ρ = density of air stream
Φ = power spectrum of fluctuating velocities

Introduction

THE wake behind an airfoil usually consists of periodic instability waves and/or coherent structures. Some profound behaviors usually appear in airfoil wake that are important to the airfoil performance. Among the most interesting behaviors related to the periodic flow in the wake are the vortex-induced vibration of the airfoil[1,2] and the lock-on phenomenon of the vortex-shedding frequency.[3] Conventionally, the research of the oscillating flows in the wake was focused on the basic flows, such as the wake behind a bluff body[4–8] or a slender body with blunt trailing edge.[9,10] For a flow passing over an airfoil, the extent of the blockage of the airfoil is decided by the angle of attack and Reynolds number based on the cross-stream length scale of the airfoil. The literature discussing the detailed behavior, dominant mechanisms, and frequency selection of the unsteady motion in the wake behind an airfoil is limited.

The wake of the airfoil at large angles of attack and Reynolds numbers was found to behave similarly to that of a bluff body.[11] The frequency selection of the flow oscillations behind a bluff body reported in the literature were commonly translated to an ordinary Strouhal number $Sr = fd/u$, where f is the flow oscillation frequency, d is the cross-stream length scale of the body, and u is the freestream velocity. Roshko[12] found that the ordinary Strouhal number remained nearly constant at 0.21, 0.18, and 0.14 for circular cylinder, 90-deg wedge, and flat plate, respectively, at Reynolds numbers between 10^3 and 10^5. The results indicated that a sharper blockage body would lead to a lower ordinary Strouhal number. Roshko[12] and Simmons[13] introduced an universal Strouhal number Sr^* based on the measured wake width d^* for several types of two-dimensional bluff bodies. They found $Sr^* = 0.163$. Roshko[12] also applied, successfully, the inviscid Kirchhoff's free streamline theory to relate the drag to the universal Strouhal number using a k function, which implied that the application of inviscid model to the bluff-body wake at large Reynolds numbers is appropriate. Levi[14] justified Roshko and Simmon's universal Strouhal law by modeling the available specific kinetic energy $u^2/2$ of the oscillating fluid with the specific mechanical energy $(2\pi f d^*)^2/2$ of the oscillator that oscillates at frequency f within the width d^*. The universal Strouhal number Sr^* thus became $1/2\pi = 0.159$. The result of the energy model seemed to be very close to that of the experiments. The Kármán-type vortex behind an airfoil at large angles of attack was discussed by Stuber and Gharib.[15] Huang and Lin[16] showed that, for a wing at angles of attack larger than 15 deg, the diverse distribution of the ordinary Strouhal numbers diminished gradually to a narrow band at chord Reynolds numbers between 0.11×10^5–1.0×10^5 and approached to a constant value of 0.12 at 90-deg angle of attack. The inviscid behavior in the unsteady wake of the airfoil at large Reynolds numbers and angles of attack was expected.

For an airfoil with a sharp trailing edge at low angles of attack without separation of surface flow, the wake was featured by the characteristics of mixing layer, which develops spatially from the instability waves of small amplitude to roll-up vortices.[16] The frequency selection of the mixing layer was different from that of the bluff-body wake because the viscous force was not negligible in the evolving process of the instability waves at the initial stage of

Received 17 September 1998; revision received 15 February 1999; accepted for publication 19 May 1999.

*Professor, Department of Mechanical Engineering, 43 Keelung Road, Sec. 4. Member AIAA.
†Graduate Student, Department of Mechanical Engineering, 43 Keelung Road, Sec. 4.

the spatially developing vortices in a free-shear layer.[17,18] The dominant mechanisms of the unsteady flow in the wake of an airfoil at low angles of attack and Reynolds numbers were inevitably different from those at large ones. Several characteristic modes of the oscillating unsteady flow at low angles of attack and Reynolds numbers were identified and found to be closely related to the boundary-layer behavior on the airfoil surfaces.[16]

The NACA 0012 wing serves as a satisfactory blockage object spanning from a slender body to a bluff body, depending on the angle of attack. The unsteady motion in the wake of the wing would hence include the characteristics of shear layer and vortex shedding. The conventional studies on the stability characteristics in the wake either theoretically assumed a laminar flow or conducted experiments in a low turbulence intensity flow. Because the effect of turbulence in the freestream on the dynamic behaviors of the unsteady structures in the wake was unclear yet, the critical limit of the turbulence intensity was undetermined. In this paper, the experimental results of the influence of the freestream turbulence intensity on the vortex shedding characteristics, such as the frequency selection and the response to the change of shedding mode, are reported.

Experimental Setup

The experiments are performed in a closed-return wind tunnel, as shown in Fig. 1 and Table 1. The size of the test section is 60 × 60 × 120 cm. The lower and upper limits of the tunnel velocity are 0.7 and 56 m/s, respectively. The rectangular wing model is made of stainless steel. The profile of the cross section is NACA 0012. A chord length of 6 cm and span of 30 cm provides an aspect ratio of 5, as shown in the subset of Fig. 1. The wing model protrudes perpendicularly through the aluminum floor of the test section and the boundary-layer thickness control plate. The leading edge of the wing model is located at 2.5C downstream from the leading edge of the boundary-layer thickness control plate and is 4.2C downstream from the exit of the wind-tunnel nozzle.

A homemade constant temperature one-component hot-wire anemometer is employed to measure the average velocity, freestream turbulence intensity, and frequency of the oscillating instabilities in the wake region. The output signals of the hot-wire anemometer are fed simultaneously to a fast Fourier transform (FFT) analyzer and a high-speed PC-based data acquisition system to perform analysis and calculations of dynamic behavior and flow statistics, as shown in Fig. 1. The hot-wire probe used is TSI 1210-T1.5, which could be used in either end-flow or cross-flow applications. The original tungsten wire is replaced by platinum wire. The wire diameter and length are 5 μm and 1.5 mm, respectively. The dynamic response corresponding to the electronic square wave test is adjusted to 20 kHz. The sampling rate and the elapse time of the data acquisition system are set to 16,000 samples/s and 2 s, respectively, for the measurement of average velocity. They are set to 32,000 samples and 1 s for the freestream turbulence intensity measurements and wake-instability detection.

To generate different turbulence intensities in the test section, fine wire-mesh screens of different mesh densities and wire diameters, as shown in the table on the top of Fig. 1 are placed between the nozzle outlet and the test section. To determine the appropriate wing model position, the flow properties on several points of (X, Y, Z) matrix in the downstream area of the mesh screen are measured with the hot-wire anemometer. Probe survey on the cross-stream plane shows homogeneity. In the streamwise direction, as shown in Fig. 2a, the decay of turbulence intensity behind the screen is fast in the first 150 mesh sizes ($X/C < -1$) and then slows down. According to Batchelor and Townsend,[19–21] the establishment period of the fully developed, almost homogeneous turbulence covers a distance to roughly 20 mesh sizes from the grid. After the establishment period, the decay of the turbulence begins. The turbulence may be considered to be in the initial period of decay up to 100–150 mesh sizes. The turbulence behind presently used generators seems to follow Batchelor and Townsend's measurements. Because the wing model is placed at 4.2C downstream from the fine-wire mesh screen (166–250 mesh sizes, depending on different screens used),

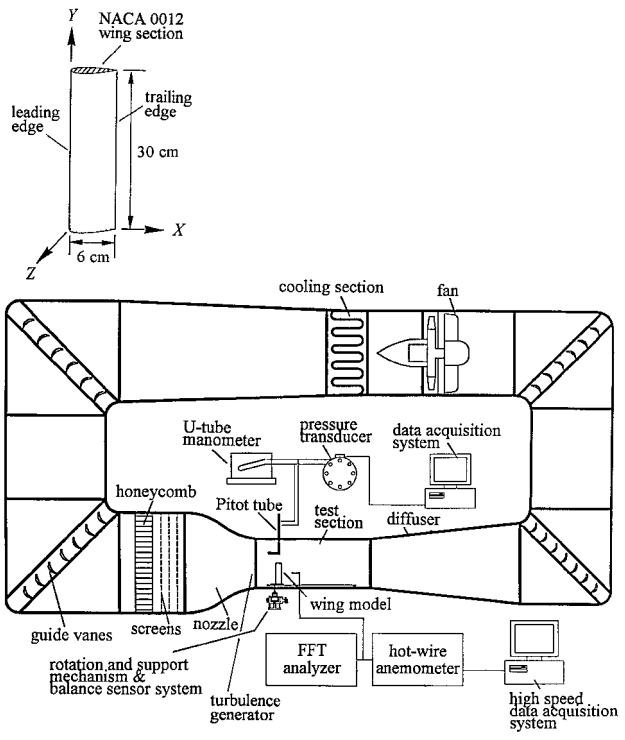

Fig. 1 Experimental setup.

Table 1 Properties of turbulence generators

Screen identification number	Mesh size M, mm	Wire diameter d, mm	M/d	Nominal freestream turbulence intensity T, %
Empty	——	——	——	0.20
24	1.058	0.25	4.232	0.40
20	1.271	0.25	5.084	0.45
18	1.410	0.35	4.029	0.50
16	1.587	0.40	3.968	0.65

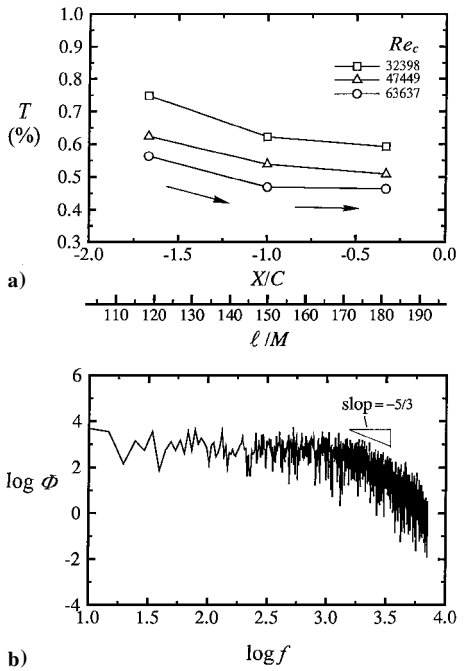

Fig. 2 Typical properties of turbulence behind fine wire-mesh screen measured in empty tunnel: a) decay of turbulence intensity T along streamwise direction on (Y/C, Z/C) = (2.5, 0) behind screen #20; b) power spectrum density function Φ, measured at (X/C, Y/C, Z/C) = (− 0.3, 2.5, 0), Re_c = 64,967. Uncertainty in T = ± 1.6%; uncertainty in Φ = ± 0.75%.

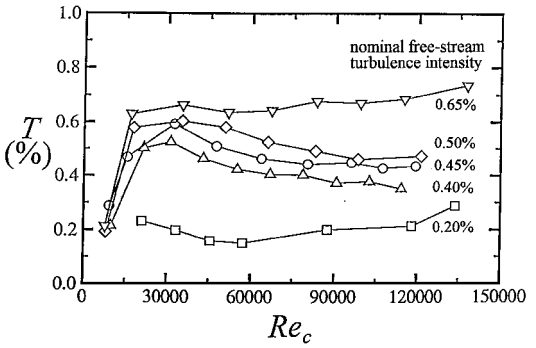

Fig. 3 Freestream turbulence intensities produced by various mesh screens. Data measured in empty tunnel at (*X/C, Y/C, Z/C*) = (0, 2.5, 0). Uncertainty in *T* = ± 1.6%.

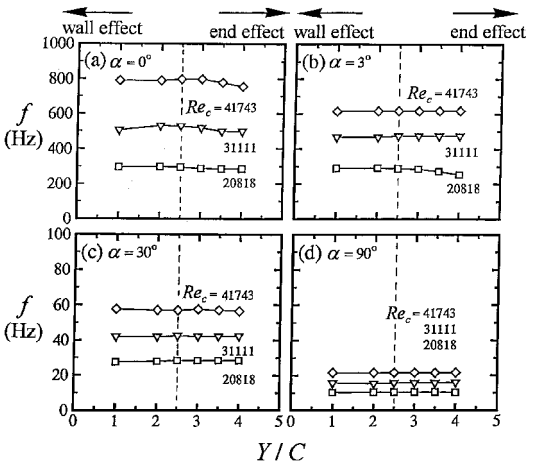

Fig. 4 Variation of instability frequency along span: a–c) measured at (*X/C, Y/C*) = (2.5, 2.5); d) measured at (*X/C, Y/C*) = (6.0, 2.5). Uncertainty in *f* = ± 0.75%.

it is beyond the establishment and initial decay periods. Because of the slow change of the turbulence with downstream distance, the turbulence would be nearly isotropic in a coordinate system moving with the mean velocity.[22,23] In the frequency domain of the typical power spectral density function, no particular peak is found, as shown in Fig. 2b. The slope $-\frac{5}{3}$ in the inertial subrange follows the law of isotropic turbulence. A total of five sets of freestream turbulence intensities are employed in this study, as shown in Fig. 3. The nominal freestream turbulence intensities 0.20, 0.40, 0.45, 0.50, and 0.65% are used in the following context.

The instabilities in the wake of the wing are detected by placing the hot-wire anemometer in the downstream area. To detect properly the frequency of the wake instabilities, the probe position is carefully adjusted in Z direction to capture the oscillation signals that are caused by the sweptover of instabilities from the trailing-edge side when the angle of attack or Reynolds number is changed. The characteristic frequency detected on the trailing-edge side is the same as that measured on the leading-edge side. Normally, the probe is positioned in the outer portion of the wake. During the experiment, the output signals of the hot-wire anemometer are monitored using an FFT analyzer through the time and frequency domains to assure the appropriation of the probe position at all times. To estimate the wall and end effects, the frequency distributions along the span direction are firstly surveyed at various angles of attack and Reynolds numbers, as shown in Fig. 4. It is apparent that at low angles of attack, the end effect makes the frequency of unsteadiness decrease appreciably when $Y/C > 3$, as shown in Figs. 4a and 4b. At large angles of attack, the end effect is not noticeable when $Y/C < 4$, as shown in Figs. 4c and 4d. The wall effect is not obvious when $Y/C > 1$ at all angles of attack, as shown in Figs. 4a–4d. The measurements thus are conducted at $Y/C = 2.5$ where both the wall and end effects are negligible. The hot-wire probe is placed in the streamwise position $X/C = 2.5$ at low angles of attack and between 2.5 and 6.0 at high angles of attack where the bluff-body effect becomes significant.

During the experiments the average velocity of the approaching flow is determined either by using a pitot-static tube in the normal velocity range or by a calibrated hot-wire anemometer in the low speed range. With the help of an on-line micropressure calibration system and careful alignment, the uncertainties of the freestream velocity measured by the Pitot tube and hot-wire anemometer are estimated to be as large as ±1.5 and ±0.8%, respectively, of the average readings. The uncertainty of the turbulence intensity measurement is within ±1.6%. The support for the wing model has a resolution of 0.015 deg. The accuracy for the hot-wire probe positioning is 10 μm. The accuracy of the shedding frequencies depends not only on the response of hot-wire anemometer but also on the record length and sampling rate of the FFT analyzer. The uncertainty of the frequency detection is estimated to be within ±0.75% of the reading in this experiment.

Results and Discussion

Characteristic Modes

From the smoke-wire visualization pictures by Huang and Lin,[16] the wake instabilities on the midchord plane behind a wing model at $Re_c = 3195$ and $T = 0.2\%$ are identified as the shear instability and vortex shedding. At very low angles of attack and Reynolds numbers, the instability waves induced by the shear effect are found in the wake.[24] The boundary layer on the suction surface at the angles of attack and Reynolds numbers where the instability waves are observed is either attached or slightly separated.[25] At medium angles of attack and Reynolds numbers, a vortex street is evolved from the suction and pressure side shear layers.[16] At large angles of attack, the large spacing between the upper and lower separated shear layers evolved from the leading and trailing edges, respectively, inhibits the direct interaction of the shear-layer instability waves.[16] The low-frequency, Kármán-type vortex street is superimposed by high-frequency, shear-layer instabilities. In the latter two regimes, the vortex street is originated from the alternative release process of the surface vortex and alleyway.[25] The term *vortex shedding* thus is applied to this type of instabilities.[24] By applying the hot-wire anemometer to the wing wake, the vortex shedding at large angles of attack can be detected by placing a hot-wire probe at far downstream locations. On the other hand, the instabilities at small angles of attack is easily detected in the near wake. The detected signals of the instability wave and vortex shedding are stated and discussed as follows.

Signal Patterns and Power Spectra

The instability wave is found in the regime of very low $u_w < 1$ m/s and $\alpha < 5$ deg. The periodic signals detected by the hot-wire anemometer in this regime contain very low amplitude of an AC component. However, the hot-wire probe positioned in the freestream area does not show periodic instability signals. The frequency of the periodic motion is low and increases slightly with the increase of freestream velocity and angle of attack. However, in the regime where the instability waves roll up and form vortex shedding,[16] the amplitude of the alternative current component of the periodic signals becomes significantly larger than that of an instability wave. It is very easy to distinguish the wave forms of hot-wire signals of the instability wave from those of vortex shedding on the oscilloscope.

Four characteristic vortex-shedding modes—laminar, subcritical, transitional, and supercritical vortex shedding—are identified in the domain of u_w and α at different freestream turbulence intensities. The typical output signals of the hot-wire anemometer and power spectra of FFT analyzer at $Re_c = 61{,}000$ and $T = 0.2\%$ are shown in Fig. 5. At $\alpha = 1$ deg as shown in Fig. 5a, the time-series signal is smooth and periodic, which is termed laminar mode. A peak is observed at $f \approx 800$ Hz in the corresponding diagram of power spectrum, as shown in Fig. 5b. At $\alpha = 3$ deg as shown in Fig. 5c, the periodic hot-wire signal is superimposed by small fluctuations, which is termed subcritical mode. A peak appearing at $f \approx 700$ Hz shows the periodic characteristics of the time-series signal, as shown in Fig. 5d. The turbulent fluctuations develop with the spatial evolution of shedding vortices. The intensity of the turbulent fluctuations amplifies and the periodicity of the vortex shedding decreases with

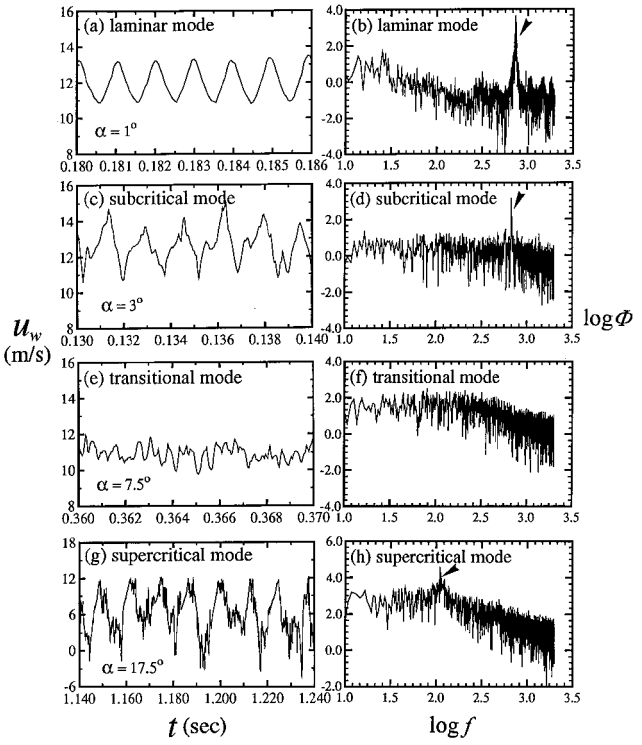

Fig. 5 Typical hot-wire signals of four characteristic modes and corresponding power spectrum density function; $T = 0.20\%$, $Re_c = 61{,}000$: a, b) $\alpha = 1$ deg; c, d) $\alpha = 3$ deg; e, f) $\alpha = 7.5$ deg; g, h) $\alpha = 17.5$ deg. Uncertainty in $u = \pm 0.8\%$; uncertainty in $\Phi = \pm 0.75\%$.

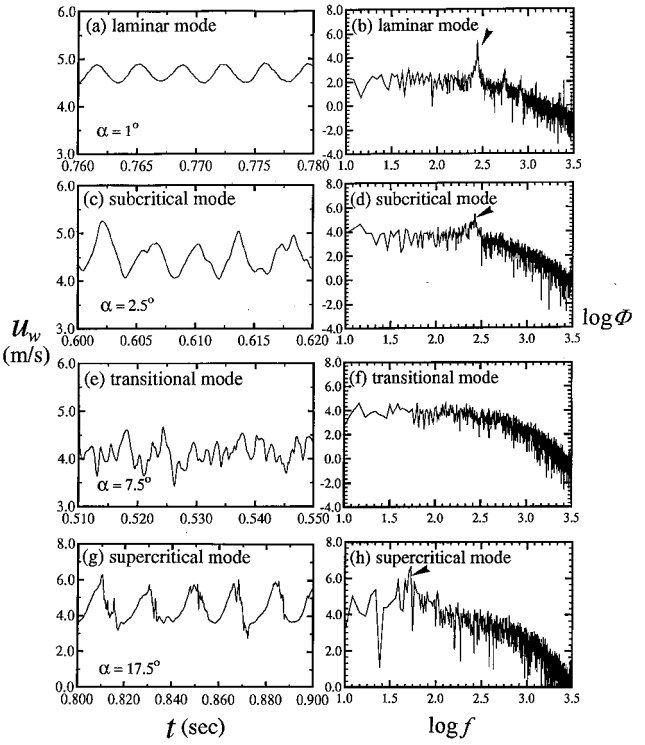

Fig. 6 Typical hot-wire signals of four characteristic modes and corresponding power spectrum density function; $T = 0.50\%$, $Re_c = 26{,}250$: a, b) $\alpha = 1$ deg; c, d) $\alpha = 2.5$ deg; e, f) $\alpha = 7.5$ deg; g, h) $\alpha = 17.5$ deg. Uncertainty in $u = \pm 0.8\%$; uncertainty in $\Phi = \pm 0.75\%$.

the increase of the Reynolds number or angle of attack. At $\alpha =$ 7.5 deg as shown in Fig. 5e, which is termed the transitional mode, the random fluctuations appear in the signal of hot-wire anemometer. No particular peak is found in the power spectrum of the velocity signals, as shown in Fig. 5f. The shed vortices lose coherency and the flow structure in the wake is disorganized, probably because of the mixing effect induced by the increased turbulence intensity. At $\alpha = 17.5$ deg as shown in Fig. 5g, which is termed the supercritical mode, the periodic hot-wire signals superimposed by large turbulent fluctuations present. The turbulent vortices are shed in the wake. A peak at $f \approx 110$ Hz in the power spectrum is observed again, as shown in Fig. 5h. The characteristic modes of the vortex shedding in the wake region are closely related to the behaviors of the boundary layer on the suction surface of the wing.[16]

The typical velocity signals and power spectrum density function at $Re_c = 26{,}250$ and $T = 0.50\%$ are shown in Fig. 6. The properties of four characteristic vortex shedding modes are similar to those at $T = 0.20\%$, except that the periodic signal of the laminar mode is a little fluctuated and the frequencies change quite a bit because of the increased freestream turbulence intensity.

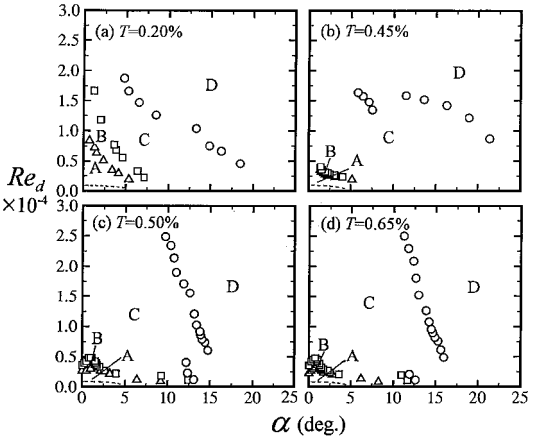

Fig. 7 Regimes of characteristic modes of wake flow in domain of chord Reynolds number and angle of attack at various freestream turbulence intensities: A, laminar; B, subcritical; C, transitional; and D, supercritical.

Regimes of Characteristic Modes

The regimes of the instability wave and vortex-shedding modes—laminar, subcritical, transitional, and supercritical—can be identified in the domain of Re_d and α, as shown in Fig. 7. The regimes of the instability wave are located at the left-lower corners below the dashed lines in Figs. 7a–7d for $Re_d < 800$ and $\alpha < 4$ deg. The critical Reynolds number decreases inappreciably with the increase of the turbulence intensity.

The regimes of laminar vortex-shedding mode appear at low Re_d and α. At $T = 0.45\%$, the boundaries identifying the characteristic modes change significantly, as shown in Fig. 7b. The changes from laminar to subcritical mode and from subcritical to transitional mode occur at lower Reynolds numbers and angles of attack. The regime of subcritical mode becomes hardly distinguishable. The upper limit of Re_d for laminar mode lowers drastically when $T > 0.45\%$. For instance, the upper limit of Re_d for the laminar mode at $\alpha = 0$ deg is about 10,000 at $T = 0.20\%$ and it decreases to 3000 at $T = 0.45\%$. The regime of the subcritical mode reduces significantly in size when $T > 0.45\%$, which can be visualized when comparing Figs. 7b–7d with Fig. 7a. Apparently, the large turbulence intensities existing in the freestream reduce the domain of periodic laminar and subcritical motions in the wake. Only at low Re_d and α can the periodic laminar and subcritical vortical motions exist when $T > 0.45\%$. At high freestream turbulence intensities, the transitional mode persists in the wake even at large Reynolds numbers. In that case the appearance of the supercritical mode is deferred until the Reynolds numbers are relatively large when $T > 0.45\%$, as shown in Figs. 7c and 7d. The patterns of characteristic regimes shown in Figs. 7c and 7d are similar; however, the boundary between the transitional and supercritical modes at $T = 0.65\%$ is located at larger angles of attack than that at $T = 0.50\%$. Larger Reynolds number or angle of attack is required to regain coherency and form turbulent organized vortices in the wake if the freestream turbulence intensity is large.

For a cylinder wake that has been extensively discussed by many investigators, different vortex shedding modes are found in different ranges of Reynolds number.[24,26] The selection of vortex shedding

modes relies heavily on the situations in the boundary layer and the wake.[26] The characteristic modes of vortex shedding in the wake of a wing model are inevitably subject to the conditions in the boundary layer and the wake. The increase in the freestream turbulence enhances the instabilities in the laminar vortex shedding so that the subcritical vortex shedding is observed at lower Reynolds numbers. Because the transition of boundary layer on the wing surface in the flow of large freestream disturbance is easier than that in the flow of low freestream fluctuation,[27] the transitional vortex shedding mode is observed at lower Reynolds numbers and angles of attack. The supercritical vortex shedding is established when the boundary layer becomes turbulent. When the freestream turbulence intensity is greater than 0.45%, the effect of freestream turbulence on the inception of turbulent boundary layer becomes saturated so that the lower boundary of the supercritical vortex shedding does not change significantly.

Frequency Selection

Strouhal and Roshko Numbers

The frequencies of the periodic unsteady motions in the wake that vary with the wind velocity are normalized and represented by nondimensional groups: $Sr_d = fd/u_w$ and $Ro_d = fd^2/\nu$, as shown in Figs. 8 and 9 for $T = 0.20$ and 0.50%, respectively.

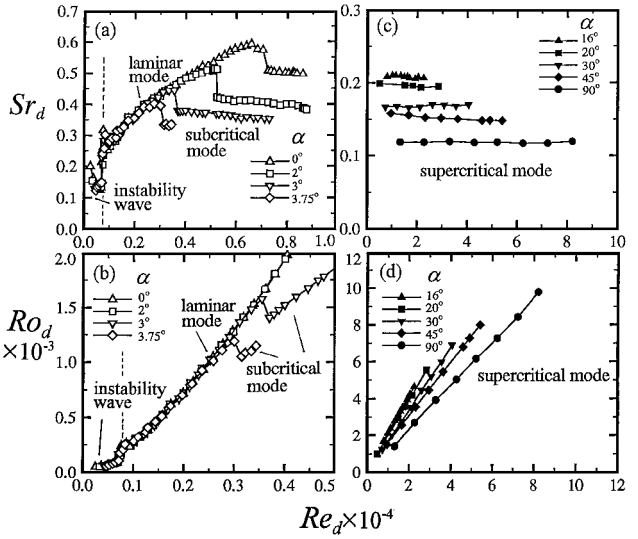

Fig. 8 Frequency selection of oscillating wake structures at $T = 0.20\%$: a, c) Strouhal number vs Reynolds number; b, d) Roshko number vs Reynolds number. Uncertainty in $Sr_d = 1.6\%$; uncertainty in $Ro_d = \pm 0.75\%$.

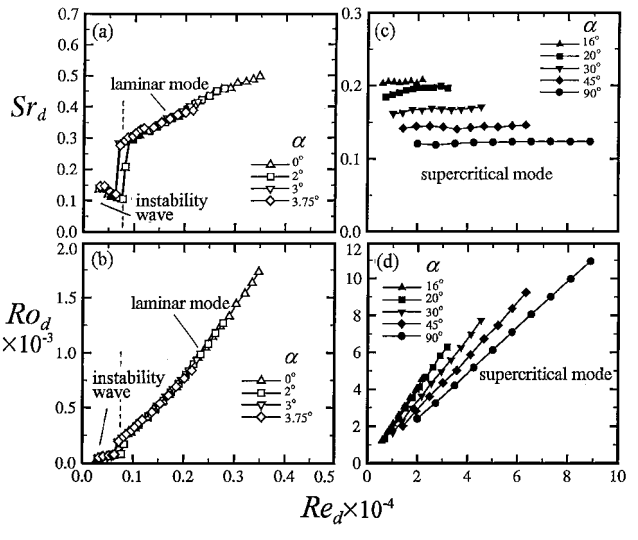

Fig. 9 Frequency selection of oscillating wake structures at $T = 0.50\%$: a, c) Strouhal number vs Reynolds number; b, d) Roshko number vs Reynolds number. Uncertainty in $Sr_d = 1.6\%$; uncertainty in $Ro_d = \pm 0.75\%$.

In the regime of instability wave, as shown in Fig. 8a, the Strouhal number decreases from 0.20 to 0.12 with the increase of Re_d at Reynolds numbers lower than about 800. At Re_d larger than about 800, the laminar mode of vortex shedding is found. The Strouhal number increases with the increase of Reynolds number. In the regimes of instability wave and laminar vortex-shedding mode the Strouhal numbers do not vary significantly for different angles of attack. The Strouhal numbers decrease rapidly to low values as the periodic motions change from laminar to subcritical mode. During the change of the characteristic modes, the turbulent fluctuations are superimposed to the periodic vortex shedding. The sudden increase of turbulence intensity enhances the effect of entrainment to enlarge the size of the vortices and thus reduces the shedding frequency. The Strouhal number thus decreases during the change of modes. In the subcritical mode, Sr_d decreases slightly with the increase of Re_d. The increase of turbulent fluctuations superimposed on the periodic motions with the increase of Reynolds number in the subcritical mode leads to the slight decrease of Sr_d.

The nondimensional group fd^2/ν is conventionally called the Roshko number and is adopted by many investigators to correlate the frequency selection of the periodic motion in the wakes to some other dimensionless parameters.[4–6,12,13] It is actually the product of Strouhal and Reynolds numbers, i.e.,

$$Ro_d = Sr_d \times Re_d = (fd/u_w) \times (u_w d/\upsilon) = fd^2/\upsilon \qquad (1)$$

which is an indication of the viscous effect on the instability frequency. In Fig. 8b, Ro_d increases from about 55 to 80 with the increase of Reynolds number from 250 to 700 in the regime of instability wave. Because the value of d does not change appreciably for α smaller than 4 deg and the viscosity ν is a constant, the frequency of the instability wave at low angles of attack in the regime $Re_d < 800$ do not vary significantly. From the similarity theory and dimensional analysis, the Roshko number is expected to remain constant if the Reynolds number is very small in the viscous-effect-dominated regime, probably in the order of 1 or 10 (Ref. 28). In the regime of $10 < Re_d < 800$, the viscous effect does not solely or completely dominate the hydrodynamic stability, so that the Roshko number increases slightly with the increase of Reynolds number.

At large angles of attack, the vortices are shed in supercritical mode where the periodic motions are superimposed by large turbulent fluctuations. Figure 8c shows the variations of Strouhal number with Reynolds number at various large angles of attack. The Strouhal numbers in the supercritical mode remain constant with the increase of Reynolds number at fixed angle of attack. The value of Sr_d decreases with the increase of angle of attack, e.g., from about 0.21 at $\alpha = 16$ deg to 0.12 at $\alpha = 90$ deg. The Strouhal number $Sr_d = fd/u_w$ is physically a parameter implying the influence of the inertial effect on the instability frequency. The constant values of Strouhal number at large Reynolds numbers delineate that the characteristics of the supercritical mode is inherently inertial effect dominated. Because the Strouhal number remains almost constant in the inertial-effect-dominated regime as shown in Fig. 8c, i.e.,

$$Sr_d = \frac{fd}{u_w} = \left(\frac{fd^2}{\upsilon}\right) \Big/ \left(\frac{u_w d}{\upsilon}\right) = \frac{Ro_d}{Re_d} = \text{const} \qquad (2)$$

The Roshko number Ro_d thus is proportional to Re_d at fixed angles of attack, as shown in Fig. 8d.

Apparently, to obtain favorable correlation, the applications of Strouhal number to large Reynolds numbers of intertial-effect-dominated regime as well as Roshko number to low Reynolds numbers of viscous-effect-dominated regime would be appropriate. At large freestream turbulence intensity $T = 0.50\%$, the influence of the viscous effect is much reduced, as shown in Fig. 9. In the regime of instability wave, the value of Sr_d at $T = 0.50\%$ in Fig. 9a is less than that at $T = 0.20\%$ in Fig. 8a, so that Ro_d in Fig. 9b is lower than that in Fig. 8b. The larger the angle of attack is, the less the viscous effect is observed, e.g., the critical value of Reynolds number when changing from instability wave to laminar vortex shedding mode at $\alpha = 3.75$ deg is smaller than that at $\alpha = 0$ deg, as shown in Fig. 9a. The viscous effect becomes insignificant when $\alpha > 4$ deg. In the regime of laminar vortex-shedding mode, the Strouhal number at $T = 0.50\%$ in Fig. 9a is much smaller than that at $T = 0.20\%$ in Fig. 8a. However, when comparing Fig. 9b with Fig. 8b, the

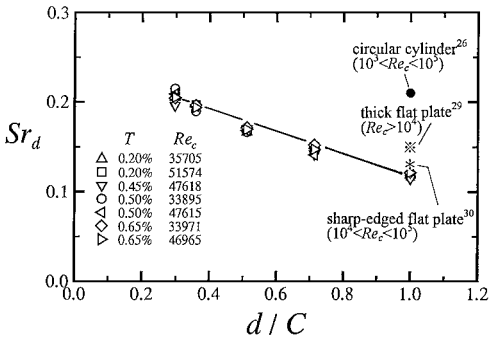

Fig. 10 Variations of Strouhal number with normalized cross-stream blockage at various freestream turbulence intensities. Uncertainty in Sr_d = 1.6%.

Roshko number does not change appreciably. The values of Strouhal and Roshko numbers in the supercritical mode at large Reynolds numbers, as shown in Figs. 9c and 9d, respectively, are not altered. The freestream turbulence intensity has no apparent effect on the vortex-shedding frequency at large Reynolds numbers because the shedding vortices of supercritical mode contain inherently high turbulence intensity. However, the effect of freestream turbulence is significant at low Reynolds-number regime of the laminar mode because the periodic signal is not superimposed by large fluctuations.

Effect of Cross-Stream Blockage

In the supercritical mode, for all freestream turbulence intensities, the Strouhal numbers remain almost the same value, decrease slowly, and eventually attain a value about 0.12 at large angles of attack, as shown in Figs. 8c and 9c. If the normalized cross-stream blockage d/C was taken as the independent variable, as shown in Fig. 10, the Strouhal number decreases almost linearly from 0.21 to 0.12 with the increase of cross-stream blockage from 0.3 to 1. For comparison, the value 0.21 is the Strouhal number measured in the wake behind a circular cylinder at large Reynolds numbers between 10^3 and 10^5 based on the cylinder diameter.[26] The Strouhal number for a vertically aligned, thick, squared-edged flat plate and sharp-edged flat plate is 0.15 and 0.13, respectively.[29, 30] It is expected that the sharpness and bluffness of the blockage in the crossflow would lead to a smaller Strouhal number. For a sharp-edged bluff body, the Strouhal number of the supercritical vortex shedding would approach a lower limit of about 0.12, no matter how large the freestream turbulence intensity is. The value 0.12 is less than the universal Strouhal number 0.159 obtained theoretically by Levi[14] for a bluff body because the physical dimension of the blockage instead of the wake width is employed in calculating the Strouhal number.

Critical Turbulence Intensity

In the regime of instability wave, the Strouhal number decreases while the Roshko number increases slightly with the increase of Reynolds number at various freestream turbulence intensities, as shown in Figs. 11a and 11b, respectively. The Strouhal and Roshko numbers at $T = 0.20\%$ are larger than those at larger turbulence intensities. The Sr_d and Ro_d have minimum values at $T = 0.45\%$. They have almost the same values at $T = 0.50$ and 0.65%. Figure 12 shows the variation of Roshko number with freestream turbulence intensity in the regime of instability wave . At all Reynolds numbers, Ro_d decreases appreciably with the increase of T to a minimum at $T = 0.45\%$, then increases rapidly to a larger value at $T = 0.50\%$. After that, the increase of freestream turbulence intensity does not seem to affect the Roshko number significantly. The increase in the freestream disturbance would superimpose an apparent viscous diffusivity[23] on the molecular viscosity. The hydrodynamic instability theory of the viscous fluid flow predicts that the increase in the viscosity would increase the stability and wave length.[31] The frequency and Roshko number thus decrease with the increase of freestream turbulence intensity. However, when $T > 0.45\%$, the effect of large turbulent fluctuation in the freestream may increase the probability of instability and overwhelm the effect of viscosity. The Roshko number thus slightly increases with the increase of T.

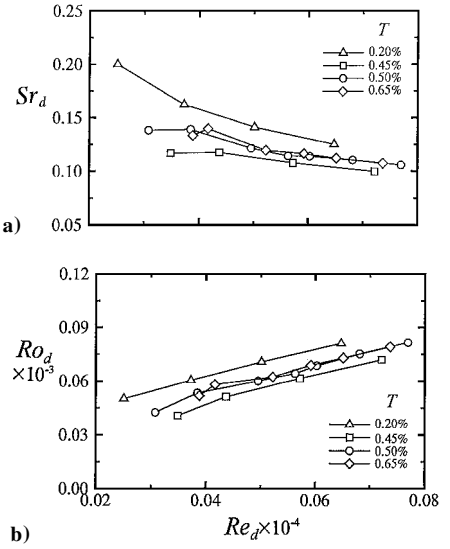

Fig. 11 Variations of a) Strouhal and b) Roshko numbers with Reynolds number at various freestream turbulence intensities in the regime of instability wave. Uncertainty in Sr_d = 1.6%; uncertainty in Ro_d = ± 0.75%.

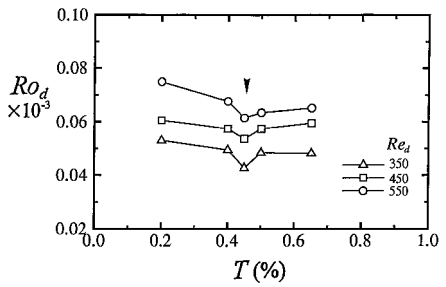

Fig. 12 Variation of Roshko number with freestream turbulence intensity at various Reynolds numbers in the regime of instability wave. Uncertainty in Ro_d = ± 0.75%.

The effects of the freestream turbulence intensity on the Strouhal number of vortex shedding are shown in Fig. 13. In the laminar and subcritical modes, as shown in Figs. 13a and 13b, respectively, the Strouhal numbers increase a little with the increase of T when $T \leq 0.45\%$, then increase rapidly when $T > 0.45\%$, and finally decrease slightly with the increase of turbulence intensity. There exists a critical value of freestream turbulence intensity between 0.45 and 0.5% for the frequency selection of the laminar and subcritical unsteady motions in the wake. The change in the characteristic surface-flow modes may contribute to existence of the critical turbulence intensity. Figure 14, which is reproduced from the results of the surface-oil flow visualization method by Lee,[28] shows the variation of the critical Reynolds number for the surface flow on the suction surface changing from separation to bubble mode. The critical Reynolds number causing the separated surface flow to reattach to the suction surface and form a separation bubble increases with the increase of the freestream turbulence intensity when $T < 0.45\%$. However, the critical Reynolds number decreases drastically when $0.45\% < T < 0.5\%$. When $T > 0.5\%$, the effect gradually saturates. At low freestream turbulence intensities, the separation point is gradually deferred downstream with the increase of T at a certain Re_d (Refs. 28, 32, and 33). The delay of separation makes the wake width smaller and thus increases the Strouhal number.[16, 18] At T between 0.45 and 0.5%, reattachment of the separated boundary layer forms a separation bubble because of the large turbulence kinetic energy containing in the freestream.[28, 32, 33] The reattachment of the turbulent boundary layer further reduces the wake width, so that the Strouhal number increases rapidly. Further increase in the freestream turbulence intensity imposes a large entrainment effect

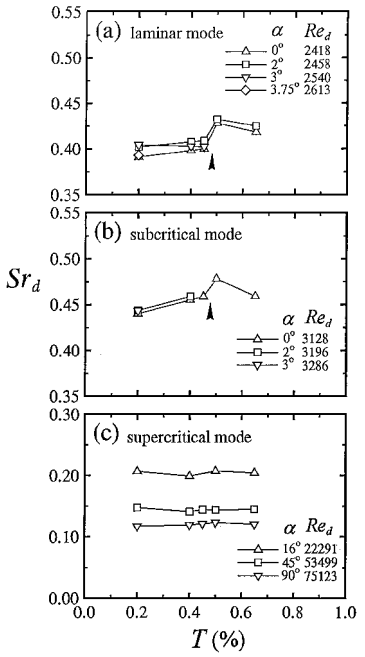

Fig. 13 Variations of Strouhal number with freestream turbulence intensity in the regime of vortex shedding. Uncertainty in Sr_d = 1.6%.

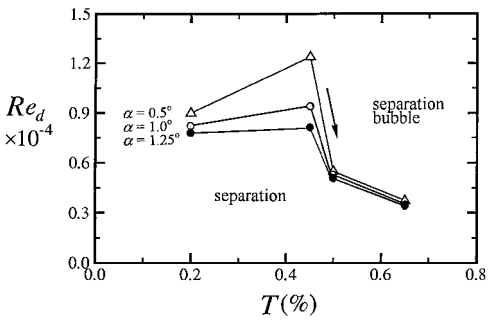

Fig. 14 Variation of the critical Reynolds number for the surface flow on the suction surface changing from separation to bubble mode. Reproduced from the results of the surface-oil flow visualization method by Lee.[28]

on the shedding vortices so that the Strouhal number decreases.[16, 18] For the supercritical mode in Fig. 13c, the Strouhal number hardly varies with the change of freestream turbulence intensity, particularly at large angles of attack. Because the surface flow does not change modes at the large angles of attack and Reynolds numbers, the freestream turbulence intensity has little effect on the supercritical vortex shedding that already contains large fluctuations on the vortices.

Conclusions

The following conclusions are drawn from the preceding discussion:

1) In the regime of very small angles of attack and Reynolds numbers, the unsteady motions in the wake are instability waves. The frequency selection is viscous-effect dominated and the Roshko number remains almost constant. In the regime of large angles of attack and Reynolds numbers, the vortex shedding is in supercritical mode. The frequency selection is inertial-effect dominated and the Strouhal number remains approximately constant.

2) The freestream turbulence has significant effects on the Strouhal and Roshko numbers in regimes of instability wave as well as laminar and subcritical vortex shedding modes because the unsteady motions in these regimes do not contain inherently large turbulence fluctuations. At large Reynolds numbers in the supercritical mode, the effect of freestream turbulence intensity is not appreciable because the vortices in this regime contain inherently large turbulence fluctuations.

3) There exists a critical value of freestream turbulence intensity between 0.45 and 0.5% for the frequency selection of the laminar and subcritical vortex shedding in the wake. The change in the characteristic surface flow modes may contribute to the dominant mechanism of the existence of critical freestream turbulence intensity.

Acknowledgment

This study was supported by the National Science Council of the Republic of China under Grant NSC 86-2212-E-011-015.

References

[1]Parker, R., "Resonance Effects in Wake Shedding from Parallel Plates: Some Experimental Observations," *Journal of Sound and Vibration*, Vol. 4, No. 1, 1966, pp. 62–72.

[2]Blevins, R. D., *Flow-Induced Vibration*, 2nd ed., Van Nostrand Reinhold, New York, 1990, pp. 43–104.

[3]Bollay, W., and Brown, C. D., "Some Experimental Results on Wing Flutter," *Journal of the Aeronautical Sciences*, Vol. 8, No. 5, 1941, pp. 313–318.

[4]Marris, A. W., "A Review on Vortex Streets, Periodic Wakes, and Induced Vibration Phenomena," *Journal of Basic Engineering*, Vol. 86, June 1964, pp. 185–194.

[5]Berger, E., and Wille, R., "Periodic Flow Phenomena," *Annual Review of Fluid Mechanics*, Vol. 4, 1972, pp. 313–340.

[6]King, R., "A Review of Vortex Shedding Research and Its Application," *Ocean Engineering*, Vol. 4, No. 2, 1977, pp. 141–171.

[7]Griffin, O. M., "Universal Similarity in the Wakes of Stationary and Vibrating Bluff Structures," *Journal of Fluids Engineering*, Vol. 103, March 1981, pp. 52–58.

[8]Griffin, O. M., "Vortex Shedding from Bluff Bodies in a Shear Flow: A Review," *Journal of Fluids Engineering*, Vol. 107, Sept. 1985, pp. 298–306.

[9]Motallebi, F., and Norbury, J. F., "The Effect of Base Bleed on Vortex Shedding and Base Pressure in Compressible Flow," *Journal of Fluid Mechanics*, Vol. 110, Sept. 1981, pp. 273–292.

[10]Vassilopoulos, K., Gai, S. L., and Petrusma, M. S., "Unsteady Flow Behind a Blunt Trailing Edge Airfoil," AIAA Paper 95-0531, 1995.

[11]Brooks, T. F., and Schlinker, R. H., "Progress in Rotor Broadband Noise Research," *Vertica*, Vol. 7, No. 3, 1983, pp. 287–307.

[12]Roshko, A., "On the Wake and Drag of Bluff Bodies," *Journal of the Aerospace Sciences*, Vol. 22, Feb. 1955, pp. 124–135.

[13]Simmons, J. E. L., "Similarities Between Two-Dimensional and Axisymmetric Vortex Wakes," *Aeronautical Quarterly*, Vol. 28, Feb. 1977, pp. 15–20.

[14]Levi, E., "A Universal Strouhal Law," *Journal of Engineering Mechanics*, Vol. 109, No. 3, 1983, pp. 718–727.

[15]Stuber, K., and Gharib, M., "Experiment on the Forced Wake of an Airfoil Transition from Order to Chaos," AIAA Paper 88-3840, 1988.

[16]Huang, R. F., and Lin, C. L., "Vortex Shedding and Shear-Layer Instability of Wing at Low-Reynolds Numbers," *AIAA Journal*, Vol. 33, No. 8, 1995, pp. 1398–1430.

[17]Oertel, H., Jr., "Wakes Behind Blunt Bodies," *Annual Review of Fluid Mechanics*, Vol. 22, 1990, pp. 539–564.

[18]Ho, C.-H., and Huerre, P., "Perturbed Free Shear Layers," *Annual Review of Fluid Mechanics*, Vol. 16, 1984, pp. 365–424.

[19]Batchelor, G. K., and Townsend, A. A., "Decay of Vorticity in Isotropic Turbulence," *Proceedings of the Royal Society of London*, Vol. 190A, 1947, pp. 535–550.

[20]Batchelor, G. K., and Townsend, A. A., "Decay of Isotropic Turbulence in the Initial Period," *Proceedings of the Royal Society of London*, Vol. 193A, 1948, pp. 539–558.

[21]Batchelor, G. K., and Townsend, A. A., "Decay of Turbulence in the Final Period," *Proceedings of the Royal Society of London*, Vol. 194A, 1948, pp. 527–543.

[22]Van Atta, C. W., and Chen, W. Y., "Correlation Measurements in Grid Turbulence Using Digital Harmonic Analysis," *Journal of Fluid Mechanics*, Vol. 34, Pt. 3, 1968, pp. 497–515.

[23]Hinze, J. O., *Turbulence*, McGraw–Hill, New York, 1975, pp. 175–320.

[24]Triton, D. J., *Physical Fluid Dynamics*, 2nd ed., Oxford Univ. Press, Oxford, 1988, pp. 22–32, 274–277.

[25]Huang, R. F., Yen, S. C., Huang, C. Y., Wu, J. Y., and Chen, R.-C., "PIV Measurements of Vortex Evolution on an Impulsively Started Wing," *Journal of Flow Visualization and Image Processing*, Vol. 6, No. 1, 1999, pp. 1–17.

[26]Lienhard, J. H., *Synopsis of Lift, Drag and Vortex Frequency Data for Rigid Circular Cylinders*, Research Div. Bulletin 300, Washington State Univ., Pullman, WA, 1966.

[27] Schlichting, H., *Boundary Layer Theory*, 7th ed., McGraw–Hill, New York, 1979, pp. 555–577.

[28] Lee, H. W., "The Flows on the Suction Surface and Instability Motions in the Wake of a Wing," Ph.D. Dissertation, National Taiwan Univ. of Science and Technology, Taipei, June 1999.

[29] Novak, J., "Strouhal Number and Flat Plate Oscillation in an Air Stream," *Acta Technica Csav*, Vol. 4, July 1973, pp. 372–386.

[30] Toebes, G. H., and Eagleson, P. S., "Hydroelastic Vibrations of Flat Plates Related to Trailing Edge Geometry," *Journal of Basic Engineering*, Vol. 83, Dec. 1961, pp. 671–678.

[31] Drazin, P. G., and Reid, W. H., *Hydrodynamic Stability*, Cambridge Univ. Press, Cambridge, England, U.K., 1981, pp. 153–245.

[32] Arena, A. V., and Mueller, T. J., "Laminar Separation, Transition, and Turbulent Reattachment Near the Leading Edge of Airfoils," *AIAA Journal*, Vol. 18, No. 7, 1980, pp. 747–753.

[33] Hunag, R. F., Shy, W. W., Lin, S. W., and Hsiao, F.-B., "Influence of Surface Flow on Aerodynamic Loads of a Cantilever Wing," *AIAA Journal*, Vol. 34, No. 3, 1996, pp. 527–532.

J. P. Gore
Associate Editor